ELSEVIER

Journal of Power Sources 111 (2002) 145–151

JOURNAL OF POWER SOURCES

www.elsevier.com/locate/jpowsour

Effect of rare earth composition on the high-rate capability and low-temperature capacity of AB_5-type hydrogen storage alloys

Hui Ye*, Baojia Xia, Wenquan Wu, Ke Du, Hong Zhang

Division of Energy Science and Technology, Shanghai Institute of Metallurgy, CAS, Shanghai 200050, PR China

Received 25 December 2001; received in revised form 12 April 2002; accepted 13 May 2002

Abstract

Effects of rare earth composition on the high-rate capability and low-temperature capacity of AB_5-type hydrogen storage alloys have been studied and analyzed with pattern recognition methods. The results show that the increase of Ce and Pr and the decrease of La and Nd concentration improve the high-rate capability and low-temperature capacity of AB_5-type hydrogen storage alloys, Ce exhibiting better favorable influences than Pr. The improvement of both high-rate capability and low-temperature capacity are mainly ascribed to the lower stability of the hydride. The alloy with the rare earth composition of $La_{0.1645}Ce_{0.7277}Pr_{0.0234}Nd_{0.0845}$ shows very good high-rate capability and low-temperature capacity.

Keywords: Hydrogen storage alloy; Metal hydride electrode; High-rate capability; Low-temperature capacity; Pattern recognition method

1. Introduction

Nickel/metal hydride (Ni/MH) battery has been rapidly developed and widely used, especially in portable electronic applications such as laptop computers, video-recorders and cellular phones [1,2].

Recently, research and development of high-power type Ni/MH battery and the one applied at low-temperature situation have become imperative [3–7]. To meet with the new power demands of hybrid electric vehicles (HEV), and some high-power applications such as power tools and new 42 V vehicle electric systems, many improvements for Ni/MH batteries, especially concerning with high-rate capability performance, have to be done [3–5]. To replace existed Ni/Cd or sealed lead–acid (SLA) batteries in some military devices, which are operated at the temperature down to 233 K [6,7], and in some civil applications at very cold areas requires to develop the environment-friendly battery working well at low temperature. Whereas, to date, the discharge performance of commercial Ni/MH battery at low temperature is poor and generally operating temperature is limited to above 253 K [7]. Thus, it is also necessary to search and develop the Ni/MH battery with superior low-temperature performance at least below 253 K.

The negative electrode active materials of Ni/MH battery mainly consist of hydrogen storage alloy. Improvement of electrochemical kinetic performance of hydrogen storage alloy is crucial to enhance the rate capability and low-temperature performance of battery. For commercial AB_5-type hydrogen storage alloy, multi-component alloying is one of the most effective techniques to tailor properties so as to meet the application requirement of batteries [1,8]. Deviating $LaNi_5$-type compound composition from stoichiometry ratio [9,10] and the addition of boron [11,12] are very effective to improve the kinetic performance of $LaNi_5$-type hydrogen storage alloys. The effects of rare earth composition on the electrochemical capacity and cycle life stability under low-rate have been widely studied [8,13–15]. However, there are few reports about the influence of rare earth composition on high-rate capability and low-temperature performance of hydrogen storage alloy.

Pattern recognition methods, such as principal component analysis (PCA), have been successfully used in the classification of chemical systems and computer-aided design of materials. PCA involves a transfer from the original feature space (e.g. the rare earth composition space) to a new space. The axes are selected to be linearly combined with original axes and orthorhombic each other. Moreover, the first axis vector shows the maximum difference among sample points and others are in sequence. As a result, the samples with different target value (e.g. high-rate capability) may be clearly classified in new space. And usually, it is reduced

* Corresponding author. Tel.: +86-21-62511070-8805; fax: +86-21-32200534.
E-mail address: yeqhui@mail.sim.ac.cn (H. Ye).

0378-7753/02/$ – see front matter
PII: S0378-7753(02)00297-5

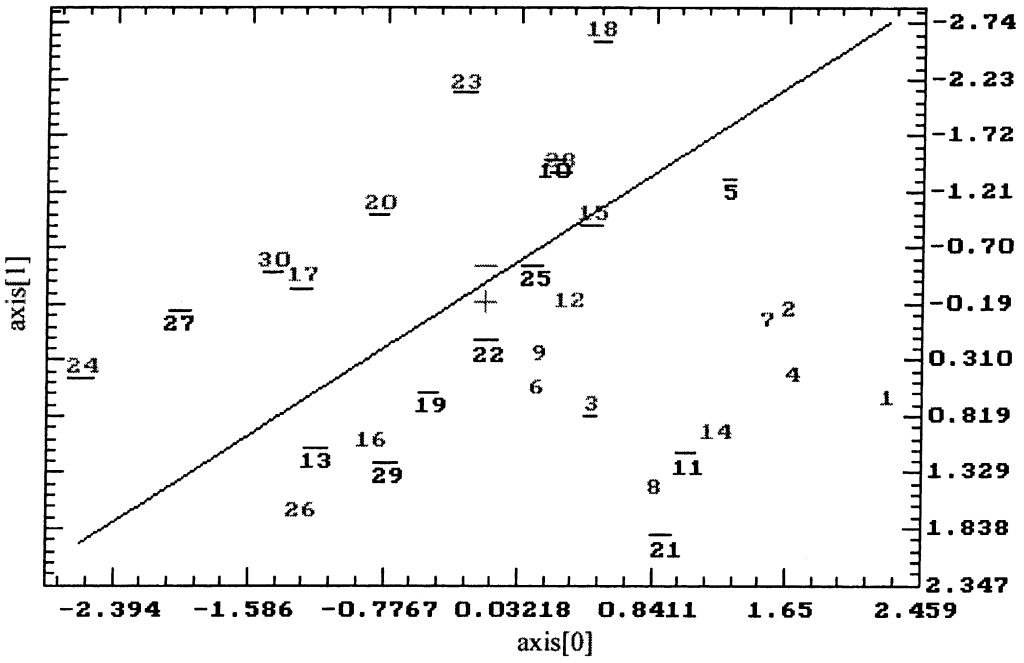

Fig. 1. Classification of alloy samples with different high-rate capability (C_H): axis[0] = $-0.0690 + 3.1656C_{La} - 0.0441C_{Ce} - 3.7279C_{Pr} + 1.0571C_{Nd}$; axis[1] = $-0.0235 + 0.5148C_{La} - 4.2083C_{Ce} + 1.0943C_{Pr} + 2.7472C_{Nd}$. The numbers with an underline: good, $C_H > 245$ mAh/g; the numbers with a bar: middle, 200 mAh/g $< C_H <$ 245 mAh/g; the numbers without an underline or a bar: bad, $C_H <$ 200 mAh/g.

to the two-dimensional axis plane (e.g. the plane constructed by axis[0] and axis[1] in the Figs. 1, 2 and 5) and there is a clear boundary line among classes with different targets. For applications, the boundary equation gives the direction how to adjust original feature to meet different classes. In our case, it means that how to adjust the composition of rare earth component to optimize the electrochemical properties. Detailed description of PCA method can be found in [16,17].

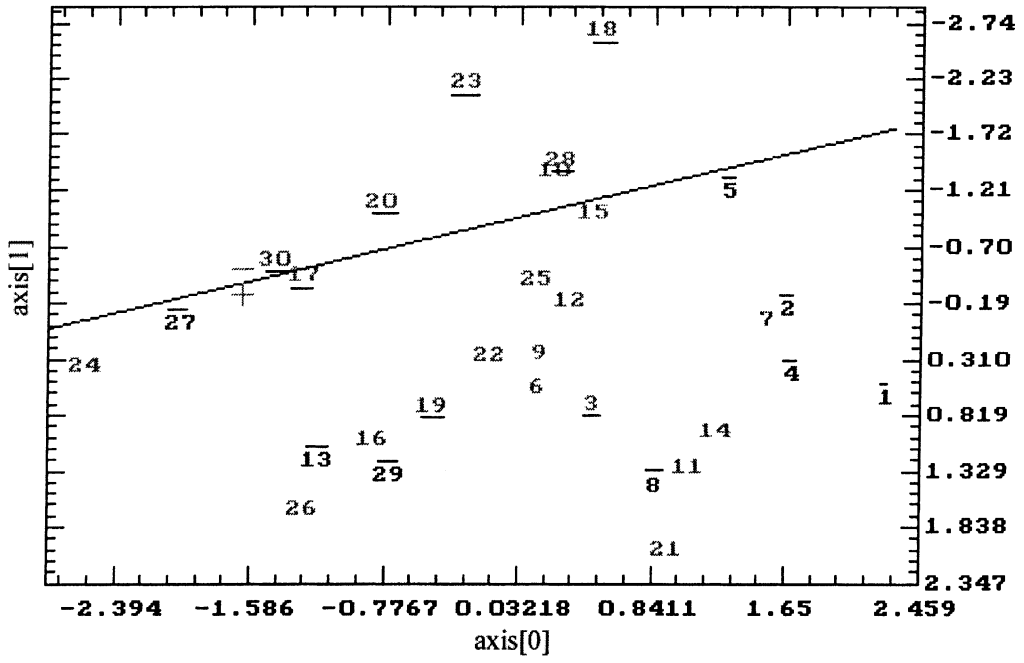

Fig. 2. Classification of alloy samples with different low-temperature capacity (C_L): axis[0] = $-0.0690 + 3.1656C_{La} - 0.04407C_{Ce} - 3.7279C_{Pr} + 1.0571C_{Nd}$; axis[1] = $-0.0235 + 0.5147C_{La} - 4.2083C_{Ce} + 1.0943C_{Pr} + 2.7472C_{Nd}$. The numbers with an underline: good, $C_L > 159$ mAh/g; the numbers with a bar: middle, 110 mAh/g $< C_L <$ 159 mAh/g; the numbers without an underline or a bar: bad, $C_L <$ 110 mAh/g.

In this paper, effect of rare earth composition (La, Ce, Pr, and Nd) on the high-rate capability and low-temperature capacity of AB_5-type hydrogen storage alloys has been studied with PCA method by using a software of KCYH developed in our institute. The thermodynamic and kinetic characteristics of hydrogen storage alloys with different rare earth composition have also been evaluated.

2. Experimental

Thirty RE $Ni_{3.55}Co_{0.75}Mn_{0.4}Al_{0.3}$ (RE representing rare earth elements) hydrogen storage alloys with different RE composition as listed in Table 1, which was designed by using the uniform distribution method, were prepared by a radio frequency levitation melting processing in a copper crucible under an argon atmosphere. La, Ce, Pr, Nd, Ni, Co, Mn, and Al with the purity over 99.5% were used as raw materials. The button ingots were re-melted three times to ensure homogeneity, then the ingots were annealed at 950 °C for 6 h. The annealed compounds were mechanically pulverized into fine powders with an average size of (ϕ) 38–75 μm for the electrochemical measurements.

The pressure-composition isotherms were measured with a Sieverts-type apparatus at 293, 313 and 333 K.

The investigated metal hydride (MH) electrode was made by uniformly mixing 0.300 g of compound powder with 1.200 g of nickel powder and then cold pressing into a pellet about (ϕ) 15.5 × 1.5 mm under pressure of 200 MPa. The electrochemical properties were measured in a standard trielectrode cell, consisted of a working electrode (MH electrode), a counter-electrode ($NiOOH/Ni(OH)_2$ electrode with 1200 mAh), and a reference electrode (Hg/HgO, OH^-). The electrolyte was a 6 M KOH solution. Discharge capacity of the hydrogen storage alloys was determined by the galvanostatic method. Discharge capacity of the alloys under 60 mA/g with the cutoff potential of −0.6 V versus Hg/HgO electrode at 293 K was defined as their maximum capacity (C_{max}). To evaluate the high-rate capability (C_H), the investigated MH electrodes were firstly charged for 72 min under 300 mA/g, then discharged under the current density of 1500 mA/g to the prescribed cutoff potential of −0.4 V versus Hg/HgO electrode at 293 K. To evaluate the low-temperature capacity (C_L), the investigated MH electrodes were firstly charged for 72 min under 300 mA/g, and then discharged under the current density of 60 mA/g to the

Table 1
Rare earth composition and electrochemical performances of hydrogen storage alloys

Number	Atomic ratio				C_{max} (mAh/g)	C_H (mAh/g)	C_L (mAh/g)	E_{mid} (V)	I_0 (mA/g)
	La	Ce	Pr	Nd					
1	0.7446	0.0548	0.0568	0.1438	339.8	159.5	116.6	−0.8896	350.021
2	0.6316	0.1969	0.1000	0.0715	341.6	156.6	115.7	−0.8973	421.991
3	0.5632	0.0341	0.3557	0.0470	340.7	247.5	159.3	−0.8923	464.89
4	0.5114	0.1608	0.0492	0.2786	335.8	192.3	113.9	−0.8997	383.873
5	0.4687	0.4125	0.0535	0.0653	337.4	200.4	116.7	−0.909	428.219
6	0.4319	0.0985	0.3522	0.1174	334.8	135.7	92.7	−0.8996	310.727
7	0.3994	0.2809	0.0053	0.3144	328.6	142.82	95.4	−0.9071	325.891
8	0.3700	0.0268	0.1910	0.4121	327.7	198.84	122.9	−0.8972	364.264
9	0.3432	0.1847	0.2911	0.181	326.9	147.2	73	−0.9044	340.806
10	0.3184	0.4488	0.2134	0.0194	326.7	223.7	100	−0.9151	374.644
11	0.2953	0.0944	0.1119	0.4984	326.8	204.14	83.09	−0.9019	387.586
12	0.2736	0.2967	0.2077	0.222	325.3	97.65	102.8	−0.9092	286.013
13	0.2531	0.0063	0.5802	0.1605	326.4	243.22	141.9	−0.8956	368.734
14	0.2337	0.1810	0.0293	0.556	327.1	176.1	51.9	−0.9068	322.395
15	0.2152	0.4488	0.1176	0.2184	322.8	246.63	94.05	−0.9155	459.056
16	0.1976	0.0773	0.4713	0.2538	324.3	176.96	75.33	−0.9008	445.447
17	0.1807	0.2905	0.5024	0.0264	330.8	246.4	166	−0.905	428.437
18	0.1645	0.7277	0.0234	0.0845	320	279.8	258	−0.9239	424.76
19	0.1488	0.1649	0.3546	0.3317	324.3	239.33	166.6	−0.9033	446.63
20	0.1338	0.4331	0.3537	0.0794	317.4	246.78	219	−0.9121	374.978
21	0.1192	0.053	0.069	0.7588	304.4	233.3	107.9	−0.9029	381.956
22	0.1051	0.2727	0.2385	0.3837	309.2	240.2	102.5	−0.9096	412.678
23	0.0914	0.6463	0.1792	0.0831	304.5	268.2	244.1	−0.9223	483.592
24	0.0782	0.1414	0.7674	0.013	321.2	262.7	108.5	−0.9019	477.012
25	0.0653	0.4087	0.1315	0.3945	303.3	239.8	58.08	−0.9144	461.068
26	0.0527	0.0240	0.5078	0.4155	309.7	119.2	71	−0.9048	372.158
27	0.0405	0.2479	0.6048	0.1067	315.7	239	142.6	−0.9101	400.69
28	0.0286	0.5952	0.0439	0.3323	310.4	261.5	235	−0.9212	480.554
29	0.0170	0.1130	0.3625	0.5075	305.4	238.36	140.4	−0.9099	420.515
30	0.0056	0.3787	0.4412	0.1744	310.4	251.3	180.4	−0.9192	395.418

The unit of E_{mid} is V vs. Hg/HgO electrode.

cutoff potential of −0.6 V versus Hg/HgO electrode at 238 K. Electrochemical micro-polarization measurements were conducted at 50% depth of discharge (DOD) and at 293 K to evaluate the electrochemical kinetic of the alloys. Discharge and micro-polarization measurements were carried out with Solartron SI1287 electrochemical interface. Before the measurements of C_H, C_L, and micro-polarization, the investigated MH electrodes were completely activated (40 cycles).

3. Results and discussion

3.1. Capacity characteristics

The electrochemical performances including maximum discharge capacity (C_{max}), high-rate capability (C_H), and low-temperature capacity (C_L) are shown in Table 1. As seen from Table 1, RE composition has less influence on C_{max} of alloys. The C_{max} of all investigated samples varies between 303 and 342 mAh/g corresponding to different RE composition. However, the value of C_H and C_L change in a very large capacity range, about 200 mAh/g, moreover, it is difficult to detect any clear variation trends for C_H and C_L with the change of RE composition. For clearly showing the influence of RE composition, here, we using 30 samples and the contents of La, Ce, Pr, and Nd listed in Table 1 as features to construct a sample matrix X, and C_H (or C_L) as target to span in a multidimensional space by the PCA method, a specific mapping pattern could be got in which the samples can be clear classified in term of the target value of C_H (or C_L).

Fig. 1 illustrates a projected linear mapping of the distribution of alloys with different C_H in the multidimensional space by the PCA method. Here, the 30 samples were classified into three grades according to the target value of C_H as follow: good, $C_H > 245$ mAh/g; middle, 200 mAh/g $< C_H <$ 245 mAh/g; bad, $C_H < 200$ mAh/g. From Fig. 1, three grades of samples except few ones are separated clearly with good samples holding the top left corner, middle ones holding the middle region, and the bad ones holding the down right corner. There is a clear boundary line between good samples and middle ones as seen in Fig. 1. According to the boundary line equation, we can obtain the criterion for the alloys with $C_H > 245$ mAh/g is:

$$2.2055 + 17.4292C_{La} - 20.5860C_{Ce} - 12.2906C_{Pr} + 18.2909C_{Nd} < 0 \quad (1)$$

combined with the boundary condition of $C_{La} + C_{Ce} + C_{Pr} + C_{Nd} = 1$. Where C_{RE} is different RE concentration expressed in atomic ratio. This criterion reveals that the increase of Ce and Pr and the decrease of La and Nd concentration improve the high-rate capability of hydrogen storage alloys. Among four RE elements, Ce shows the most significant influence on the high-rate capability of alloys.

Fig. 2 illustrates a projected linear mapping of the distribution of alloys with different C_L in the multidimensional space by the PCA method. Here, the samples were also classified into three grades according to the target value of C_L as: good, $C_L > 159$ mAh/g; middle, 110 mAh/g $< C_L <$ 159 mAh/g; bad, $C_L < 110$ mAh/g. Seen from Fig. 2, the distribution of middle samples and bad one is somewhat disordered. However, the good samples ($C_L > 159$ mAh/g) stand out from other ones with a boundary line in the Fig. 2. According to the boundary line equation, we can obtain the criterion for the alloys with $C_L > 159$ mAh/g is:

$$12.1893 + 21.8114C_{La} - 56.4127C_{Ce} - 2.9743C_{Pr} + 41.6788C_{Nd} < 0 \quad (2)$$

combined with the boundary condition $C_{La} + C_{Ce} + C_{Pr} + C_{Nd} = 1$. This criterion also reveals that the increase of Ce and Pr and the decrease of La and Nd concentration improve low-temperature capacity C_L, yet Ce, and Nd concentration show much larger influence on the value of C_L and the influence of Pr concentration is rather inconspicuous.

The electrochemical performances of the hydrogen storage alloy are intrinsically determined by its micro-structure, thermodynamic and kinetic characteristics under the application environment. Of course, the change of effective specific surface of the alloy resulting from pulverization during charge/discharge process will also affect its performances. The XRD analysis results of Adzic et al. [13] and Valoen et al. [14] and our investigated samples 15, 18, and 25, all indicate that stoichiometric AB_5-type hydrogen storage alloys with different RE composition have hexagonal single phase. Of course, the substitution of La with Ce, Pr, and Nd will change the unit cell volume of the hexagonal phase due to different atomic radii of RE elements, and will further influence the other characteristics of alloys. At following text, we will analyze the influence of RE composition on electrochemical capacity mainly in the term of thermodynamic and the electrochemical activity of alloys.

3.2. Thermodynamic characteristics

For an electrochemical Ni/MH cell, the transfer of hydrogen from the bulk of hydrogen storage alloy to the surface may become the controlling-step during the discharge process of negative electrode, especially under large current density or at low temperature. Iwakura et al. [18] reported that the lower the stability of hydride, the higher the Einstein diffusion coefficient D^*, which is proportional to the coefficient of hydrogen D_H. The stability of metal hydride can be characterized by the enthalpy of hydride decomposition on the base of the Van't Hoff equation:

$$\ln P_{eq} = -\frac{\Delta H^{des}}{RT} + \frac{\Delta S^{des}}{R} \quad (3)$$

Where ΔH^{des}, ΔS^{des} are the enthalpy and entropy of desorption 1 mol of gaseous hydrogen from the hydride phase and R is the gas constant. And the equilibrium hydrogen pressure (P_{eq}) can be got from pressure–composition isotherms (P–C-I) measured with a Sieverts-type apparatus. Nevertheless, The P–C-I measurement of alloys is really time-consuming. Here, we use the open-state potential of the alloy at 50% DOD, E_{mid}, to evaluate the stability of its hydride.

The potential of the hydrogen storage alloy versus Hg/HgO electrode can be expressed as Eq. (4) according to Nernst equation using parameters adopted by Iwakura and Asaoha [19]:

$$E = E^0(H_2O/H_2) - E^0(Hg/HgO) + \frac{RT}{2F} \ln \frac{\alpha(H_2O)}{\gamma(H_2)P_{eq}(H_2)} \quad (4)$$

Here, E is the test value of potential of the alloy (versus Hg/HgO, 6 M KOH), R the gas constant, T the temperature (K), F Faraday's constant, $\gamma(H_2)$ the fugitive coefficient of hydrogen (about 1.00058), $\alpha(H_2O)$ is the activity of water. Combining Eqs. (3) and (4), we can get Eq. (5):

$$E = E^0(H_2O/H_2) - E^0(Hg/HgO) + \frac{RT}{2F} \ln \frac{\alpha(H_2O)}{\gamma(H_2)} - \frac{T\Delta S}{2F} + \frac{\Delta H}{2F} \quad (5)$$

Eq. (5) shows that there is a linear relationship between the potential of MH electrode and the enthalpy of MH decomposition. This will be further confirmed by the experimental results of partial samples as below.

The open-state potential of investigated MH electrodes at 50% DOD (E_{mid}) were tested and also listed in Table 1. P–C-I curves of partial samples (1, 6, 26, 22, 25, 23, and 18 with gradually more negative E_{mid}) were measured with a Sieverts-type apparatus. The equilibrium hydrogen pressures corresponding to the composition of 3 hydrogen atoms per molecule (H/M) were used to draw the Van't Hoff plots, which are shown in Fig. 3. The equilibrium hydrogen pressure of sample 1 at 298 K was unavailable due to the limit of apparatus. Fig. 3 indicates that the alloy with more negative E_{mid} also exhibit higher plateau pressure at the same test temperature. According to Eq. (3), the ΔH^{des} of each alloy can be got from Fig. 3. Then the relationship between E_{mid} and ΔH^{des} of alloys are plotted out in the Fig. 4. Fig. 4 clearly shows that the more negative potential of the alloy, the lower value of ΔH^{des}, indicating that it is reasonable to use E_{mid} to evaluate the stability of hydride. The more negative of E_{mid}, the lower stability of corresponding MH is.

Fig. 5 illustrates a projected linear mapping of the distribution of alloys with different E_{mid} in the multi-dimensional space by the PCA method. Here, the 30 samples were classified into three grades according to the target value of E_{mid} versus Hg/HgO as: unstable, $E_{mid} < -0.9100$ V; middle, $-0.9100\,V < E_{mid} < -0.9000$ V; stable, $E_{mid} > -0.9000$ V. There is a discriminable distribution of samples in the Fig. 5. According to the boundary line between unstable samples and middle ones seen in Fig. 5, the criterion for the unstable alloys with $E_{mid} < -0.9100$ V is:

$$3.7958 + 12.2583C_{La} - 23.1736C_{Ce} + 9.8118C_{Pr} + 0.2982C_{Nd} < 0 \quad (6)$$

combined with the boundary condition $C_{La} + C_{Ce} + C_{Pr} + C_{Nd} = 1$. This criterion reveals that the increase of Ce concentration and the decrease of La, Pr, and Nd concentration lead to more negative E_{mid}, thus, decrease the stability of corresponding hydride. Here, Ce element shows

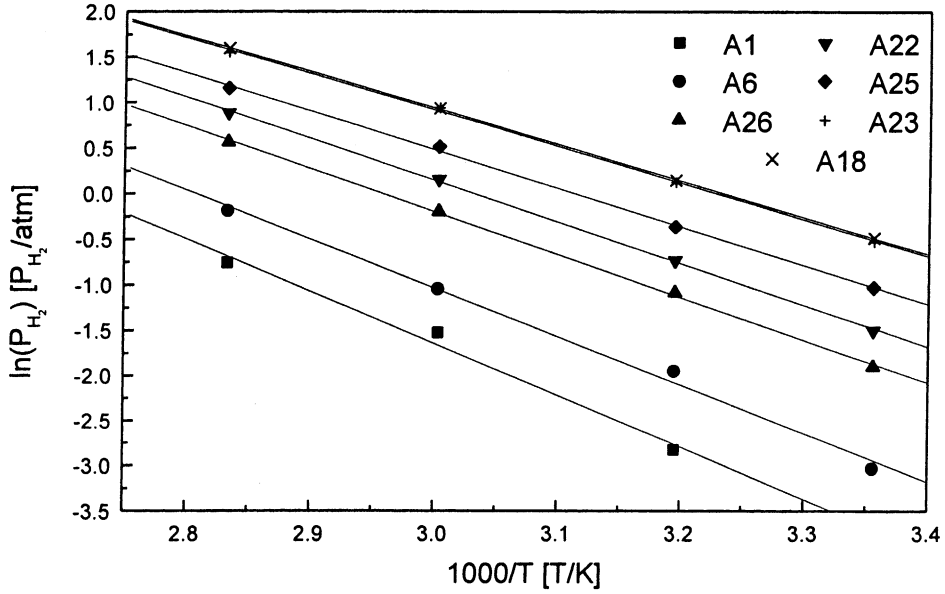

Fig. 3. Van't Hoff plots of hydrogen storage alloys (samples 1, 6, 26, 22, 25, 23, and 18 with gradually more negative E_{mid}).

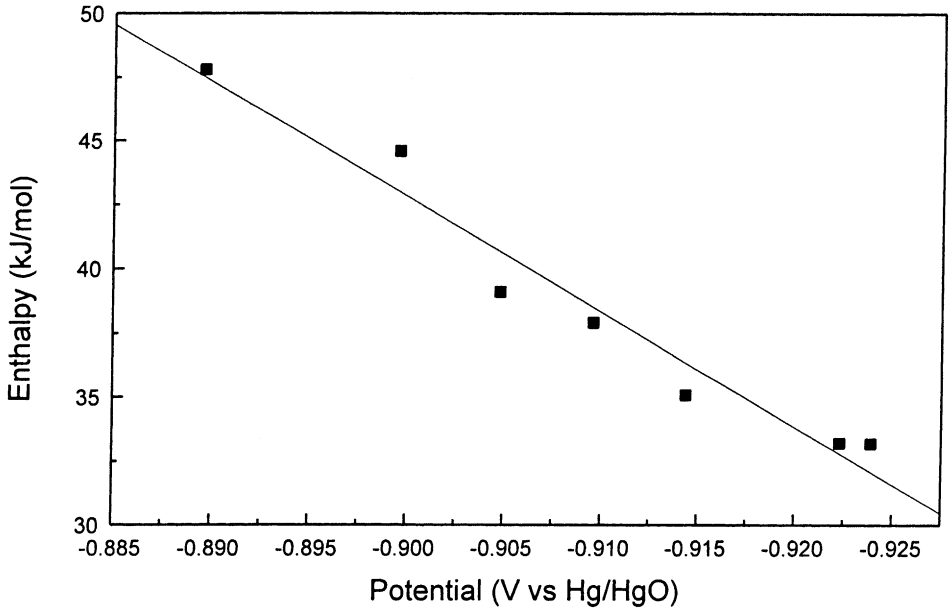

Fig. 4. Relationship between the open-state potential of the alloys at 50% DOD (E_{mid}) and their decomposition enthalpy (small square from left to right corresponding to samples 1, 6, 26, 22, 25, 23, and 18 with gradually more negative E_{mid}).

a dominant role on decreasing the stability of hydride, which is consistent with the results of Valoen et al. [14]. As to the reason why Ce can show prominent effect on the stability of hydride is still insufficient.

Compared of Figs. 1, 2 and 5, there is a good consistency between the value of C_H or C_L and the stability of the hydride. The lower stability of the hydride corresponding to higher hydrogen diffusion coefficient in the alloy, thus, facilitates the transfer of hydrogen in the bulk and thus, increase the discharge efficiency of alloy under high-rate current or at low temperature, which results in high value of C_H or C_L. The benefit effects of Ce on the high-rate capacity and low temperature may mainly ascribe to it remarkably lowering the stability of alloys. Sample 18 with highest Ce

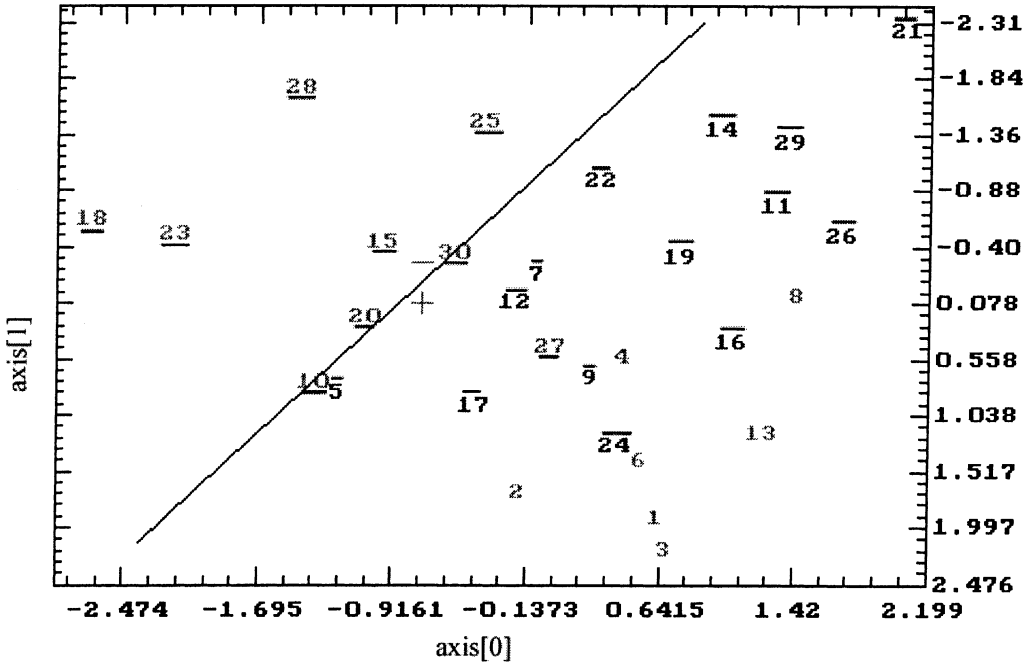

Fig. 5. Classification of alloy samples with different open-state potential of investigated MH electrodes at 50% DOD (E_{mid}, V vs. Hg/HgO) axis[0] = $-0.0235+0.5148C_{La} - 4.2083C_{Ce} + 1.0943C_{Pr}+2.7472C_{Nd}$; axis[1] = $0.0706 + 3.0756C_{La} - 1.3778C_{Ce} + 1.5262C_{Pr} - 3.6754C_{Nd}$. The numbers with an underline: unstable, $E_{mid} < -0.9100$ V; the numbers with a bar: middle, $-0.9100\,V < E_{mid} < -0.9000$ V; the numbers without an underline or a bar: stable, $E_{mid} > -0.9000$ V.

content shows the best high-rate capability and low-temperature capacity, which confirms the above analysis. The adverse effects of La or Nd can also be partially ascribed to their effects of increasing the stability of hydride; whereas, it seems that the favorable effect of Pr on C_H and C_L cannot be explained only by the stability of hydrides.

3.3. Electrochemical activity

The exchange current density (I_0) for the hydride electrode reaction is used to character the electrochemical activity for charge transfer at the metal/electrolyte interface and it can be obtained by the following formula [20]:

$$I_0 = \frac{RT}{FR_d} \quad (7)$$

Here, R_d, F, R and T are the charge transfer resistance, Faraday constant, gas constant and absolute temperature, respectively.

The exchange current densities of investigated MH electrodes at 50% DOD were tested by micro-polarization method and also listed in the Table 1. We cannot get any clear correlation between exchange current density and RE composition even by the PCA method. Thus, it seems inappropriate to explain the influence of RE composition on C_H and C_L only from the view of the electrochemical activity of the alloys. Whereas, it is not to downplay the effects of the electrochemical activity on the C_H and C_L, the increase of exchange current density (I_0) consequentially does favor to the increase of C_H and C_L. As seen from Figs. 1 and 2, sample 3 shows large deviation from the optimum region though it has higher C_H and C_L value, which can be explained well by its quite larger I_0. Combining the increase of the electrochemical activity and the decrease of the stability, it will be more favorable to increase the value of C_H and C_L, samples 23 and 28 exemplifying this point.

4. Conclusion

(1) Pattern recognition method has been successfully used to optimize the rare earth composition of hydrogen storage alloy. It is clearly shown that the increase of Ce and Pr concentration and the decrease of La and Nd concentration improve the high-rate capability and low-temperature capacity of AB_5-type hydrogen storage alloys. Ce shows significant favorable influence on the high-rate capability and low-temperature capacity.

(2) The open-state potential of the alloy at 50% DOD, E_{mid}, can be conveniently used to evaluate the stability of its hydride. The more negative of E_{mid}, the lower stability of corresponding MH. The improvement of both high-rate capability and low-temperature capacity are mainly ascribed to the lower stability of the hydride. The good electrochemical activity of alloy further enhances these performances. The favorable role of Ce element is attributed to its dominant influence in decreasing the stability of hydride. Whereas, the mechanism of Pr has to be studied further.

(3) The alloy with the rare earth composition of $La_{0.1645}Ce_{0.7277}Pr_{0.0234}Nd_{0.0845}$ shows the best high-rate capability and low-temperature capacity, thus, it is very suitable for high-power Ni/MH battery or the Ni/MH battery used at very low temperature (238 K).

References

[1] J.J.G. Willems, Philips J. Res. Suppl. 39 (1984) 1.
[2] T. Sakai, I. Uehara, H. Ishikawa, J. Alloys Comp. 293–295 (1999) 762.
[3] H. Ye, H. Zhang, Adv. Eng. Mater. 3 (2001) 481.
[4] P. Gifford, J. Adams, D. Corrigan, S. Venkatesan, J. Power Sources 80 (1999) 157.
[5] G. Gutmann, J. Power Sources 84 (1999) 275.
[6] J.K. Erbacher, J. Power Sources 80 (1999) 265.
[7] T.B. Atwater, P.J. Cygan, F.C. Leung, J. Power Sources 91 (2000) 27.
[8] J.J. Reilly, G.D. Adzic, J.R. Johnson, T. Vogt, S. Mukerjee, J. McBreen, J. Alloys Comp. 293–295 (1999) 569.
[9] Y. Fukumoto, M. Miyamoto, M. Matsuoka, C. Iwakura, Electrochim. Acta 40 (1996) 845.
[10] H. Ye, H. Zhang, J.X. Chen, T.S. Huang, J. Alloys Comp. 308 (2000) 163.
[11] H. Ye, H. Zhang, W.Q. Wu, T.S. Huang, J. Alloys Comp. 312 (2000) 68.
[12] H. Ye, Y.X. Huang, J.X. Chen, H. Zhang, J. Power Sources 103 (2001) 293.
[13] G.D. Adzic, J.R. Johnson, J.J. Reilly, J. McBreen, S. Mukerjee, J. Electrochem. Soc. 142 (1995) 3429.
[14] L.O. Valoen, A. Zaluska, L. Zaluski, H. Tanaka, N. Kuriyama, J.O. Strom-Olsen, R. Tunold, J. Alloys Comp. 306 (2000) 235.
[15] J. Guo, C.H. Li, H.L. Liu, N.Y. Chen, J. Electrochem. Soc. 144 (1997) 2276.
[16] D.E. Rumelhart, J.L. Mcclelland, Paralleled Distributed Processing, MIT Press, Cambridge, MA, 1986.
[17] N. Chen et al., Application of Pattern Recognition Methods, Science Publication, China, 2000.
[18] C. Iwakura, T. Oura, H. Inoue, M. Matsuoka, Y. Yamamoto, J. Electroanal. Chem. 398 (1995) 37.
[19] C. Iwakura, T. Asaoha, Nippon Kagaku Kaishi 8 (1988) 1482.
[20] P.H.L. Notten, P. Hokkeling, J. Electrochem. Soc. 138 (1991) 1877.